



ORIGINAL ARTICLE

The effective adsorption of arsenic from polluted water using modified Halloysite nanoclay



Naif S Aljohani ^{a,b}, Yasar N Kavit ^c, Radwan K Al-Farawati ^c, Saeed Saad Alelyani ^c, Mohammed I Orif ^c, Yasser A Shaban ^c, Saedah R Al-Mhyawi ^d, Enas H Aljuhani ^e, Mohamed Abdel Salam ^{f,*}

^a Department of Environmental Sciences, Faculty of Meteorology, Environment and Arid Land Agriculture, King Abdulaziz University, P.O. Box 80208, Jeddah 21589, Saudi Arabia

^b Saline Water Conversion Corporation, P.O. Box 5968, Riyadh 11432, Saudi Arabia

^c Department of Marine Chemistry, Faculty of Marine Sciences, King Abdulaziz University, P.O. Box 80207, Jeddah 21589, Saudi Arabia

^d Department of Chemistry, College of Science, University of Jeddah, P.O. Box 80337, Jeddah 22233, Saudi Arabia

^e Department of Chemistry, Faculty of Applied Science, Umm Al-Qura University, Makkah, Saudi Arabia

^f Department of Chemistry, Faculty of Science, King Abdulaziz University, P.O. Box 80200, Jeddah 21589, Saudi Arabia

Received 15 September 2022; accepted 2 February 2023

Available online 8 February 2023

KEYWORDS

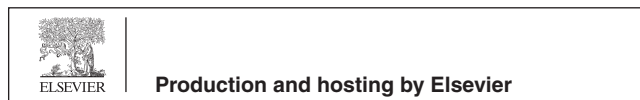
Halloysite nanoclay;
As (III);
Polluted water;
Adsorption;
Kinetics

Abstract The presented research applied the modified Halloysite nanoclay to boost the adsorption efficacy of heavy metals from the water. To improve As (III) adsorption effectiveness from water, the study assessed the characteristics of the prepared materials and improved the experimental conditions. The study was optimized the experimental condition with a dosage of 1 g/L, contact time of 90 min, the solution pH of 8, and the initial concentration of 5 ppm of As (III). The optimization was performed in distilled water and later the experiments were conducted in the real polluted water. The modified Halloysite nanoclay's physical characteristics were investigated using techniques like X-ray diffraction, scanning and transmission electron microscopy, Fourier transform infrared spectroscopy, and surface area analysis. The experimental result shows the adsorption efficiency of 82.4 % of As (III) at the optimized condition during the usage of modified Halloysite nanoclay. To create a suitable mathematical model for a better description of the interactions between pollutants and solid adsorbents, it is helpful to analyze the process

* Corresponding author.

E-mail addresses: masalam16@hotmail.com, mabdelsalam@kau.edu.sa (M. Abdel Salam).

Peer review under responsibility of King Saud University.



kinetically. The removal process of As (III) was studied kinetically and the observation shows the pseudo-second order kinetics.

© 2023 The Authors. Published by Elsevier B.V. on behalf of King Saud University. This is an open access article under the CC BY-NC-ND license (<http://creativecommons.org/licenses/by-nc-nd/4.0/>).

1. Introduction

Environmental poisoning of water sources around the world is causing increasing worry, as are the health implications on humans (Wen et al., 2019). Inappropriate use has harmed and degraded nearly all natural water supplies, putting the world's population at risk of severe drinking water shortages. In addition, the water ecosystem and geological cycles have been affected as a result of this. According to a WHO report, nearly 600 million people globally, especially in developing countries, lack access to safe drinking water (WHO, 2006). The massive discharge and leaching of heavy metals has contaminated the aquatic environment in recent decades (Du et al., 2014). As a result of their high persistence, detrimental effects on the neurological system, and even concern resulting from their accumulation at certain levels, heavy metal poisoning of the environment has recently drawn increased attention (Ciopec et al., 2013). The presence of arsenic (As) in water intended for human consumption and wastewater poses a serious threat to human health and the environment (Costa, 2019). It has long been known that arsenic is a human carcinogen that causes a variety of malignancies, including skin, lung, bladder, liver, and prostate cancers (Costa, 2019; Asere et al., 2019). Arsenic distribution in various water beds around the world causes a slew of environmental and societal issues. Because of arsenic's severe toxicity, the US Environmental Protection Agency (US EPA) reduced the arsenic drinking water standard from 0.05 mg/L to 0.01 mg/L in 2006. The maximum allowable amount of As in drinking water has been set at 0.01 mg/L by the World Health Organization (WHO). Arsenic is found in natural waters primarily as an inorganic species in two forms: arsenite As (III) and arsenate As (V). As (III) is more common in groundwater than As (II) (V). As (III) is more toxic to humans than As (V) and is more sensitive to mobilization (Han et al., 2007). The most of the treatment procedures are more effective for high initial arsenic concentrations (typically greater than 100 mg/L), but they leave residual arsenic concentrations that exceed the water quality standards required in most countries (Mohan et al., 2007). Hence, the scientific community is still working on new technologies to remove residues of arsenic from drinking water, wastewater, and industrial effluents in order to attain safe limits (Negrea et al., 2014).

Several types of processes, including coagulation and precipitation, electro dialysis, membrane separation, photocatalysis and chemical catalysis, bioremediation, adsorption, disinfection, and hybrid processes, have been tested for the separation of various pollutants from water, including microbial contaminants (Sharma and Bhattacharya, 2017). Adsorption is the most eco-friendly, cost-effective, and straightforward of all of these techniques. Many publications (Asere et al., 2019; Chakraborty et al., 2022; Manna et al., 2018; Peechattukudy and Dhoble, 2017; Rodriguez- Narvaez et al., 2017; Yagub et al., 2014; Rahman et al., 2021; Rahman and Raheem, 2022) have well demonstrated the efficacy of various adsorbents for pollutant separation. Furthermore, nanoparticles have been tested for other domestic utilities as well as for the removal of arsenic from tainted water to make it potable. The increased characteristics of functionalized nanomaterials (Chalasanani and Vasudevan, 2012) brought about by their synergistic and cooperative effects make them appealing. Arsenic has recently been removed from contaminated water using acetate functionalized zinc oxide nanoparticles (Singh et al., 2013). A new hybrid polyacrylamide chromium oxide (PACO) for the adsorption of arsenic from water was also recently introduced by Rahman and Haseen (2014). The development of a new adsorbent with qualities and characteristics that suggest a high adsorption capacity for metal ions is

required based on the profits of adsorption. As a result, raw materials such as drinking water treatment sludge and clay should be studied for synthesis of effective adsorbents for the removal of As. Although activated carbon has been the most widely used for pollutant adsorption, it is still pricey when compared to other low-cost adsorbents (Babel and Kurniawan, 2003) like clay minerals. Because of their inexpensive cost, natural abundance, and environmental friendliness, clay minerals have also been frequently used as adsorbents. Clays are up to 20 times less expensive than activated carbon (Bhattacharyya and Gupta, 2008). Clays also have a moderate specific surface area and a high cation exchange capacity (Bhattacharyya and Gupta, 2008; Long et al., 2013). Nanoclays (NC) are a type of nano-adsorbent substance that can be used to remove a wide range of pollutants. Nanoclays are a new type of adsorbents made up of nano-dimensionally coated mineral silicates that are low-cost, non-hazardous, long-lasting, and have a high surface reactivity (Abdel-Fadeel et al., 2022). Nanoclays, such as Halloysite Nanoclay, have recently been investigated as a possible adsorbent for the removal of heavy metals and organic dyes from various aquatic environments (Aljohani et al., 2021; Aigbe et al., 2022; Novikau and Lujaniene, 2022). Even though numerous studies has been reported for the removal arsenic from the water, the usage of the low cost and ecofriendly materials were limited due to the restricted removal efficiency. This makes more novelty on the material used in the present study. The present study aims to remove As (III) compounds from the polluted water using modified Halloysite nanoclay. The study was evaluated the characterization of the prepared materials and optimized the experimental conditions to achieve the better adsorption efficiency. Furthermore, the modified nanoclay showed better adsorption properties and superior ability to remove the As (III) from the water bodies.

2. Materials and methods

2.1. Characterization

The morphology of the HS and MHS nanoclay was examined using a JEOL JEM-1230 transmission electron microscope (TEM). An X-pert pro diffractometer from Philips was used to obtain X-ray diffraction (XRD) patterns. The automatic gas sorption system A NOVA 3200e was used to measure the specific surface area (Quantachrome, Boynton Beach, FL, USA).

2.2. Adsorption experiment

The adsorption experiment has carried out in a water samples collected from the polluted water located at Al-Arbaeen lagoon. Al-Arbaeen lagoon is situated on the Red Sea shoreline in Jeddah. With two loops spanning nearly N–S and a network of contacts connecting the interior basins to the open sea, Al Arbaeen lagoon features a more intricate T-shape. El Rayis and Moammar (1998) assert that there is a continuous interchange of water with the open sea at the top two meters of the surface layer. On rare occasions, bottom water will regenerate in rough and stormy conditions (Orif et al., 2017).

To determine the As (III) adsorption capability on Halloysite nanoclay (HS) and 8-hydroxyquinoline-modified HS

nanoclay, arsenic adsorption studies were carried out (MHS). In 50 mL centrifuge tubes with 20 mL of an As (III) solution and a predetermined volume of HS or MHS, several experiments were conducted. 0.1 M HCl or 0.1 M NaOH were used to change the pH of the mixture. On a shaker spinning at 350 rpm, all the solutions were mechanically stirred. The initial As (III) solution's pH was not changed during the adsorption kinetics and adsorbent dose studies in order to represent a system with no outside influences, and it was fixed to be at a pH of 3. Each experiment was carried out at room temperature. To ascertain the equilibrium contact duration and maximum adsorption capacity, kinetic studies were carried out at intervals ranging from 0 to 150 min. Through testing several adsorbent dosages between 0.25 and 1.25g, the most effective adsorbent dosage was found. At pH levels ranging from 3 to 9, experiments studying how pH affects adsorption capacity were carried out. After the pH studies, initial As (III) concentration trials were conducted with As (III) initial concentrations ranging from 0.25 mg/L to 10 mg/L at a pH of 8. Then the resultant solution is filtered using the filter paper and the filtrate were tested using ICP-AES.

The adsorption capacity, q_t , at a specific time t and the percent removal of arsenite were calculated based on the following equations:

$$q_t = \frac{(C_0 - C_t) \times V}{W} \quad (1)$$

$$\text{Percentage of Removal} = (C_0 - C_t) / C_0 \times 100 \quad (2)$$

where C_0 (mg/L), and C_t (mg/L) are respectively the initial and equilibrium As (III) concentrations, V (L) is the volume of the solution, and W (g) is the weight of the adsorbents HS or MHS.

2.3. Determination of point of zero charge

This study used the salt addition method to estimate the point of zero charge (PZC) of the adsorbent (Bakatula et al. 2018; Rahman and Varshney, 2021). For this, 25 mL of 0.1 M NaNO₃ in different pH (3–10) solutions were taken in volumetric flasks, and 0.2 g of prepared adsorbent was then added. By adding 0.1 M HCl or NaOH solutions, the pH of the liquids was regulated. After 24 h, the pH (pH_f) of the solutions was assessed. Plotting the initial pH (pH_i) readings against the Δ pH (pH_i - pH_f) values were used to calculate the PZC.

3. Results and discussion

3.1. Characterization

The Fig. 1 shows the TEM characterization of the MHS nanoclay. It is evident that the MHS was made up of a hollow tube-like structure. The TEM image presented in Fig. 1 revealed that the modified HS nanoclay have diameters of 40–60 nm, lumens in the range of 10–15 nm, and lengths within the range of 100–900 nm. The images also show the cross aggregates between the nanotubes brought on by static electric charges. It is evident from the surface morphology that it is a lamellar material made up of various arrays of cleaved sheets (Thommes, 2010; Zhu et al., 2016). An increase in the contact area and active sites for the adsorption of heavy metals from

effluents was eventually achieved with the aid of the modification of HS nanoclay, which favors the creation of many cavities and a rather loose surface (Zhang and Wang, 2015). The EDX pattern of MHS nanoclay is shown in the Fig. 2 and the atomic % of each element is listed in the Table 1. It can be seen that the EDX of MHS show the presence of aluminum, silicon, carbon, nitrogen and oxygen. It is very clear from the Fig. 2 that synthesized sample are free from other elemental impurities. The reflection peaks at diffraction angles of $2\theta = 11.8^\circ, 19.84^\circ, 24.53^\circ, 35.01^\circ, 36.68^\circ, \text{ and } 38.05^\circ$, which correspond to the reflection planes (001), (110), (002), (122), (200), and (131), are explained by the XRD pattern of MHS nanoclay in Fig. 3 (Senoussi et al., 2016). The modified halloysite nanoclay was found to have a basic spacing (001) of $7.49 (2\theta = 11.81^\circ)$.

By using FTIR analysis, the surface functional groups of MHS nanoclay were described. The Fig. 4 shows the FTIR spectra of the pristine and modified HS nanoclay. Both spectra had the characteristic peaks of the HS nanoclay at $3696 \text{ cm}^{-1}, 3629 \text{ cm}^{-1}, \text{ and } 1654 \text{ cm}^{-1}$ and are assigned to the O—H stretching of the inner-surface hydroxyl groups, the O—H stretching of inner hydroxyl groups, and deformation of water, respectively. In addition, the presence of the strong —OH absorption band at 3433 cm^{-1} was more pronounced for the modified HS nanoclay due to the presence of 8-HQ at the nanoclay. Also, a band was observed at 1730 cm^{-1} for the modified HS nanoclay may be attributed to conjugated C=O stretching vibrations due to the presence of 8-HQ at the nanoclay surface. Also, the bands appears at 1763 cm^{-1} to $1458 \text{ cm}^{-1}, 1384 \text{ cm}^{-1}, 814 \text{ cm}^{-1}, \text{ and } 671 \text{ cm}^{-1}$ correspond to the characteristic quinoline stretching vibrations (Weerasuriya et al., 2017; Shao et al., 2011; Kosa et al., 2012). Also the vibrations in the ranges 1384 cm^{-1} to 1465 cm^{-1} and 1095 cm^{-1} to 1280 cm^{-1} correspond to the aromatic amine resonance frequencies for C—N bond and C—O stretching frequencies, respectively (Weerasuriya et al., 2017; Shao et al., 2011; Kosa et al., 2012). According to Fig. 5, which categorizes the N₂ adsorption/desorption isotherms for MHS as type III isotherms, the specific surface (BET) is $72.5 \text{ m}^2/\text{g}$. The smaller mesopores and higher surface area of HS permitted capillary condensation.

3.2. Effect of dosage

Fig. 6 for HS and MHS at various loadings illustrates the impact of the adsorbent dosage on the removal of As (III). Fig. 6 shows that 1 g/L of the modified HS dosage is enough to allow for the quantitative adsorption of As (III). With increasing modified HS dosage, more As (III) is eliminated. There are more active sites available for adsorption due to the rise in the percentage caused by the increase in the amount of existing solid phase (Kavil et al., 2018; Abdel-Fadeel et al., 2022). It is obvious that adsorption onto MHS is caused by the 8-hydroxyquinoline species, which offer complementary adsorption sites for As (III) species, because adsorption on HS is far less significant than that on MHS. The greater adsorbent surface and more available metal ion adsorption sites are the likely causes of the increase in adsorption with adsorbent dosage (Maleki et al., 2015). The overlapping or aggregation of adsorption sites, which lengthens the diffusion path and

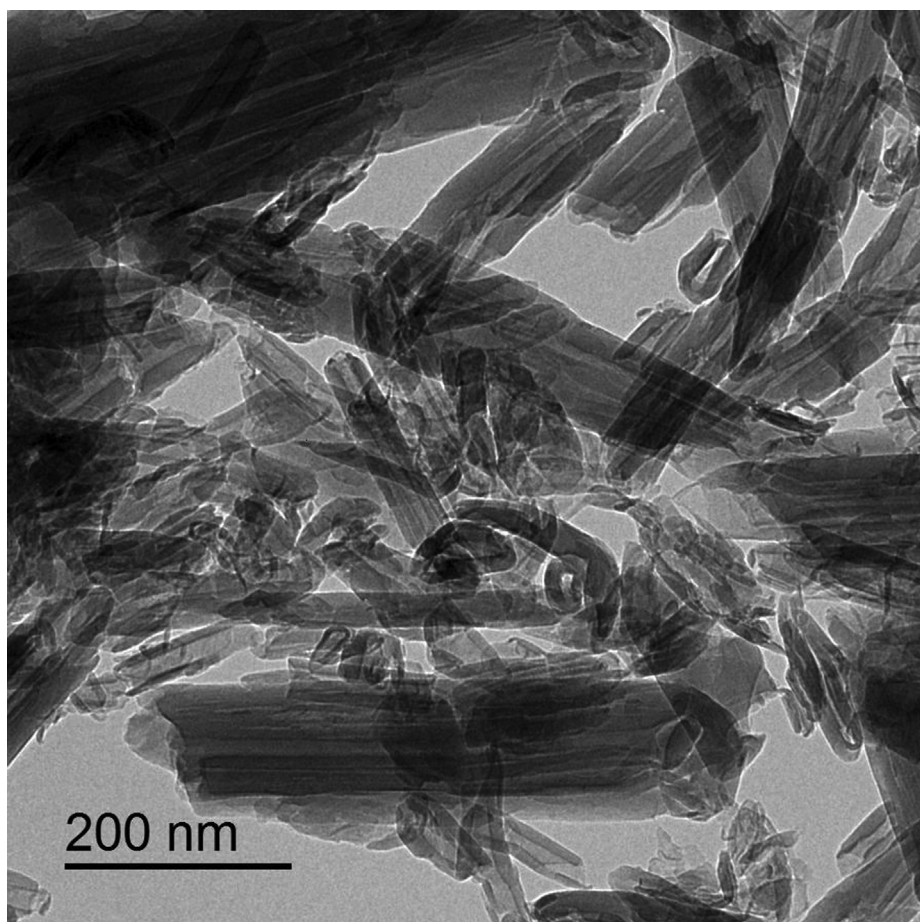


Fig. 1 TEM characterization of the MHS nanoclay.

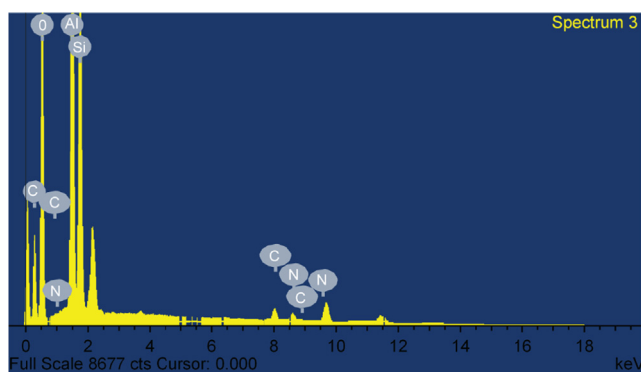


Fig. 2 The EDX pattern of MHS.

Table 1 The weight and atomic % of elements in MHS.

Element	Weight %	Atomic %
C	27.56	36.50
O	52.92	52.61
Al	10	5.89
Si	8.27	4.68
N	1.25	0.31

reduces the overall adsorbent surface area that is available to the metal ions, may be to blame if the adsorption capacity reduced beyond the limit of adsorbent dosage (Crini et al, 2008). In the present study the equilibrium was reached with a dosage of 1 g/L.

3.3. Effect of contact time

Equilibrium between the adsorbent and the solution's solute must be attained for adsorption to be fully effective. Therefore, a specific amount of time is needed for the equilibrium's contacts in order to guarantee that adsorption is attained. The contact time is the length of time needed to reach equilibrium. Numerous writers have investigated how contact time affects adsorption. Their findings demonstrated that the rate of metal ion adsorption rises over time, reaching an optimal value at which point no further metal ion removal occurs (Azouaou et al, 2010; Martinez et al, 2006; Montazer-Rahmati et al, 2011). The Fig. 7 shows the effect of contact time on the adsorption of As (III) using HS and MHS nanoclay. The present study achieved an adsorption efficiency of 83.6 % with the MHS nanoclay over the contact time of 150 min. During this experiment the parameters like pH, the dosage of adsorbent and the temperature were kept constant. The adsorption up to 90 min were quite fast and afterwards it was showing a slight elevation in the adsorption for both HS and MHS nanoclays. The maximal adsorption capacity attained by the

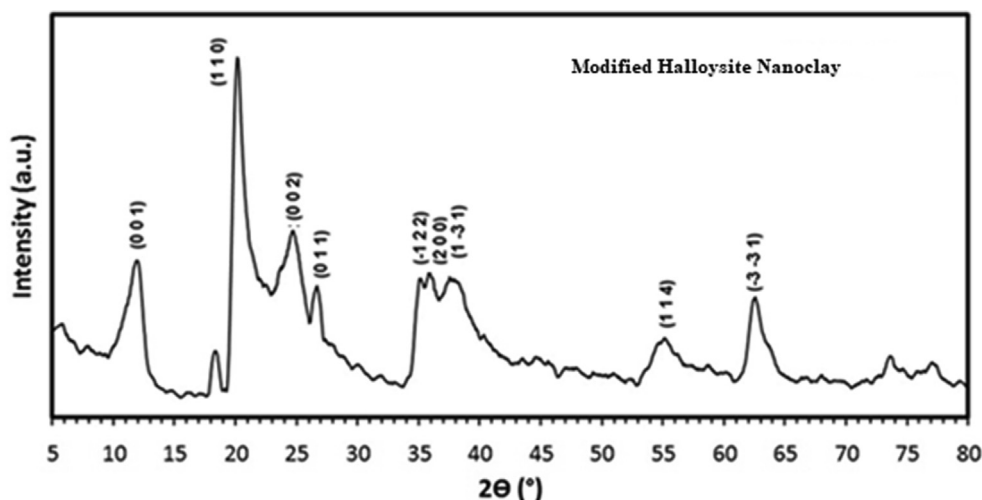


Fig. 3 XRD pattern of MHS nanoclay.

adsorbent under the operating conditions is reflected in the quantity of metal ions adsorbed at the time of contact. Adsorption is observed to be nearly constant beyond the equilibrium time, which is explained by the availability of empty surface sites during the initial stages of adsorption and the difficulty of filling the empty sites after equilibrium has been reached due to the repellent forces between the heavy metal molecules on the HS/MHS and bulk solution (Alley, 2007). The similar observations were noted in elsewhere (Selomulya et al, 1999; Attia et al, 2010; Brahmaiah et al, 2015).

3.4. Effect of pH

In the process of heavy metal adsorption, the pH level of the metal solution is crucial. It makes a significant adsorption capacity contribution. The aqueous solution's behavior and the surface attachment locations are both impacted by pH (Ushakumari and Madhu, 2013). The adsorbent surface charge has an impact on pH. The pH affects the surface charge, ionization potential, and distribution of metal ions in the adsorbent (Park et al, 2010). The 8-hydroxyquinoline (8-HQ), also known as 8-quinolinol or oxine, is a well-known monoprotic, bidentate chelating agent. It is a compound that contains an oxygen donor atom and a nitrogen donor atom that can both bind to metal atoms. When the pH of an adsorbent surface is reduced, the H^+ ions that are present in high numbers neutralize the negatively charged surface, reducing the barrier to diffusion and increasing the rate of adsorption. The effect of solution pH on this study is shown in the Fig. 8. The study was done in a range of pH between 3 and 9. In comparison to acidic medium, overall heavy metal removal values in alkali solutions were significantly greater. Fig. 8 illustrates this phenomenon, showing that metal ion adsorption is minimal in the acidic zone ($pH = 3$), increases with rising pH, and reaches its highest value at $pH = 8$. These findings suggest that the ability of the material to adsorb metal ions was lowered by protonation of more basic pyridine-type nitrogen in the quinoline rings. The high concentration of hydroxyl ions (OH^-) in the solution may be the cause of the decrease in metal ion absorption at pH levels higher than 8 (Ghaemy et al, 2015). Lowering the positive charges of amino groups reduces the pH values, which enhances adsorption

behavior (Maleki et al, 2015). In line with prior arsenite adsorption experiments (Yuh-Shan, 2004; Ho and McKay, 1998; Weber and Morris, 1963), the current investigation found that As (III) adsorption increased with increasing pH up to $pH = 9$. At a pH less than 8, attraction and repulsion are ineffective against neutral H_3AsO_3 because the adsorption process may be regulated by H_3AsO_3 surface complexation that causes deprotonation or dissociation (Bhowmick et al, 2014). Adsorption occurs most frequently in the neighborhood of $pH = 8$. Moreover, the point of zero charge of the adsorbent was found to be 8 (Fig. 9). The balancing effect of the As (III) solution at high pH caused the reaction mixture's pH to rise above 8, which likely caused a decrease in adsorption and the onset of precipitation/coagulation (Tandon et al, 2013).

3.5. Effect of initial concentration

The initial concentration of the solution affects the rate of adsorption. Adsorption experiments from the past have demonstrated that at lower concentrations, the rate of adsorption increases (Shaban et al, 2019; Alfarawati et al, 2020; Kavil et al, 2020). The deposit of metal at the interface between the solid and liquid phases is the broad definition of the mass transfer process known as metal adsorption. In order to investigate this, the initial metal concentration was varied between 0.25, 1, 3, 5, 7, and 10 ppm of As (III). The effect of initial concentration for the adsorption of As (III) in the present study is shown in the Fig. 10. It is clearly observed that the lower concentration was adsorbed quickly compared to the higher level of As (III). This is due to the fact that most metal ions remained unadsorbed when the concentration was high due to saturation of the adsorption sites (Azouaou et al, 2010). Because there was more adsorbent surface area available at lower concentrations, the rate of adsorption increased (Kumar et al, 2010).

3.6. Adsorption kinetics

Adsorption rate predictions offer crucial details about adsorption mechanisms. The experimental data at different adsorption durations corresponding to the changes in adsorption

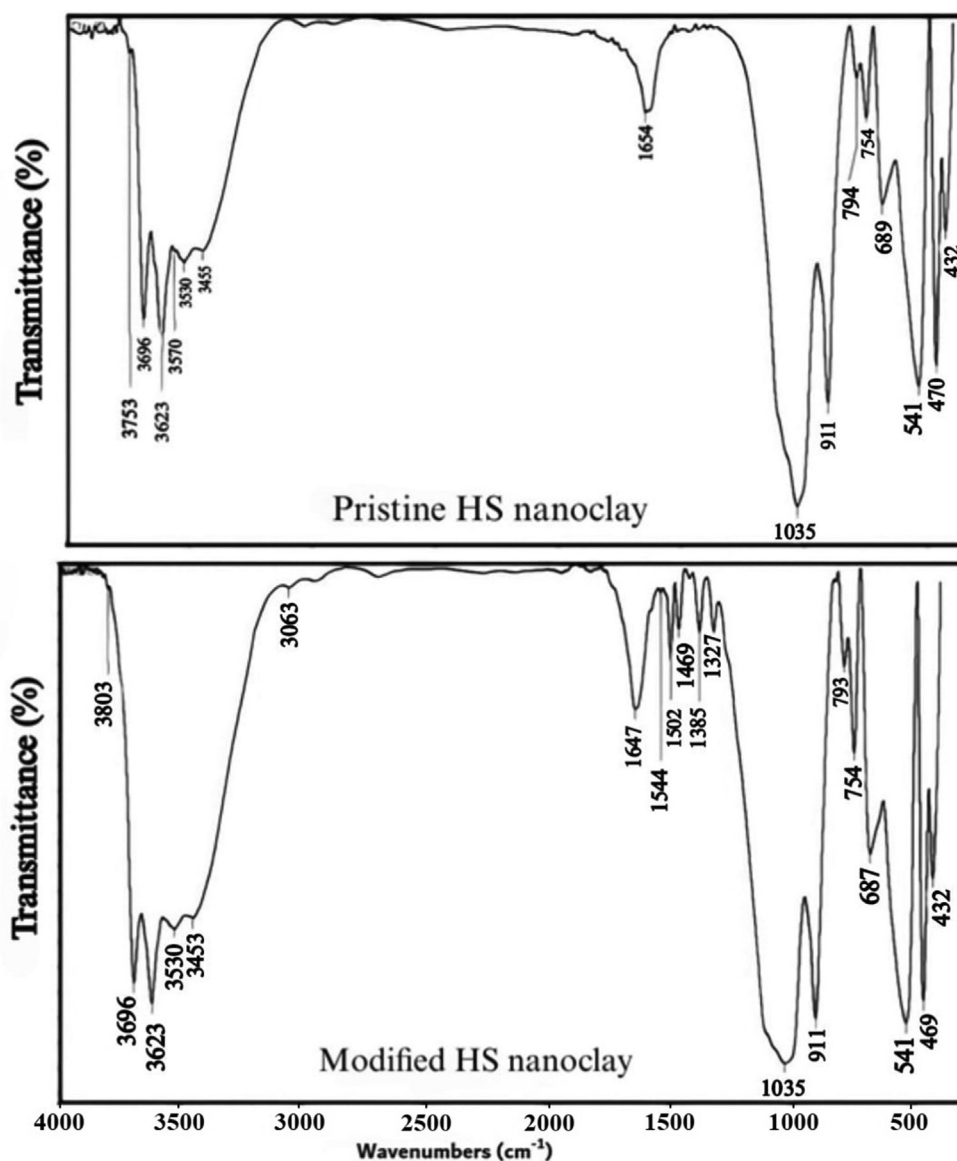


Fig. 4 FTIR spectrum of the pristine and modified HS nanoclay.

capacity were fitted using the pseudo-first-order model to assess the adsorption mechanism onto MHS. The following equations was used to determine the pseudo-first-order model,

$$\frac{dq_t}{dt} = k_2(q_e - q_t)^2$$

$$\frac{t}{q_t} = \frac{1}{k_2 q_e^2} + \frac{t}{q_e}$$

Where q_e (mg/g) is the quantity of As (III) adsorbed at equilibrium, q_t (mg/g) is the amount of As (III) adsorbed at a specific time t (min), and k_2 (g/mg min⁻¹) is the pseudo-second-order reaction rate. The terms k_2 and q_e can be calculated from the intercept and slope of the (t/q_t) vs t plot, respectively.

In order to create the proper adsorbent materials for environmental remediation, it is helpful to investigate the process kinetically in order to develop an adequate mathematical model for a better description of the interactions between pol-

lutants and solid adsorbents. The experimental removal capabilities, or the quantity of metal ions adsorbed from the desalination outfall sample by MHS nanoclay (q_t), are shown to vary with interaction time in Fig. 11. The adsorption/removal of As (III) by MHS nanoclay was discovered to reach equilibrium within 90 min, and further extending the contact period had little effect on the removal capabilities. The Lagergren pseudo-first-order (PFO) kinetic model was used to kinetically analyze the adsorption experiment results displayed in Fig. 12. The current data demonstrate the superior values of the PSO kinetic models' regression coefficients when compared to the PFO kinetic models, demonstrating the suitability of the PSO kinetic model for explaining the removal of As (III). The pattern is shown in the Fig. 13. The adsorption process was also partially modeled by the Elovich model, as shown in Fig. 13, which also shows that the adsorption sites were heterogeneous and that a variety of activation energies occurred during the adsorption process. Given that this model had the highest R^2 , a comparison of the R^2 values clearly demonstrates

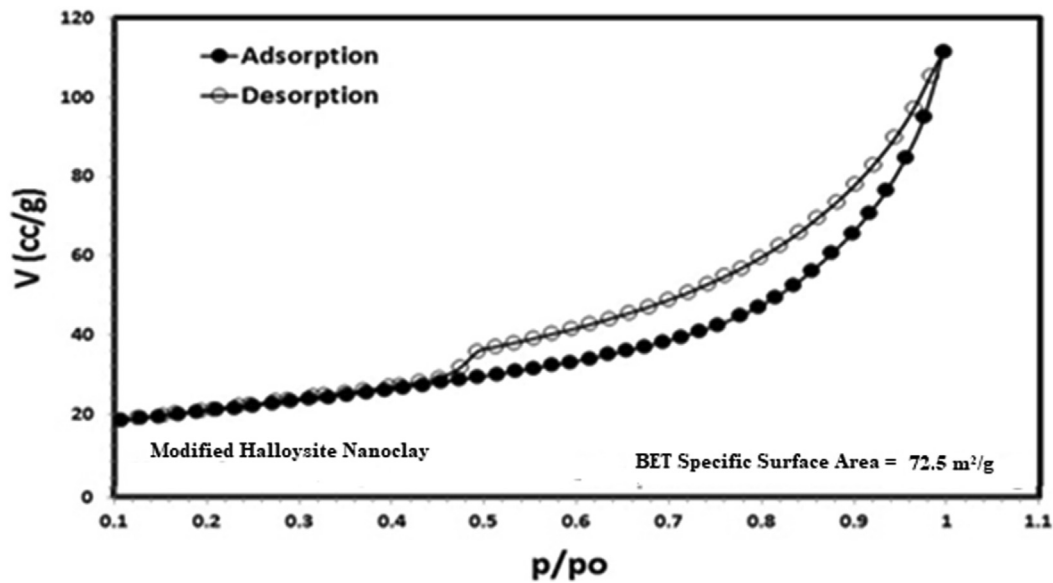


Fig. 5 BET surface area of Modified Halloysite nanoclay at 77 K.

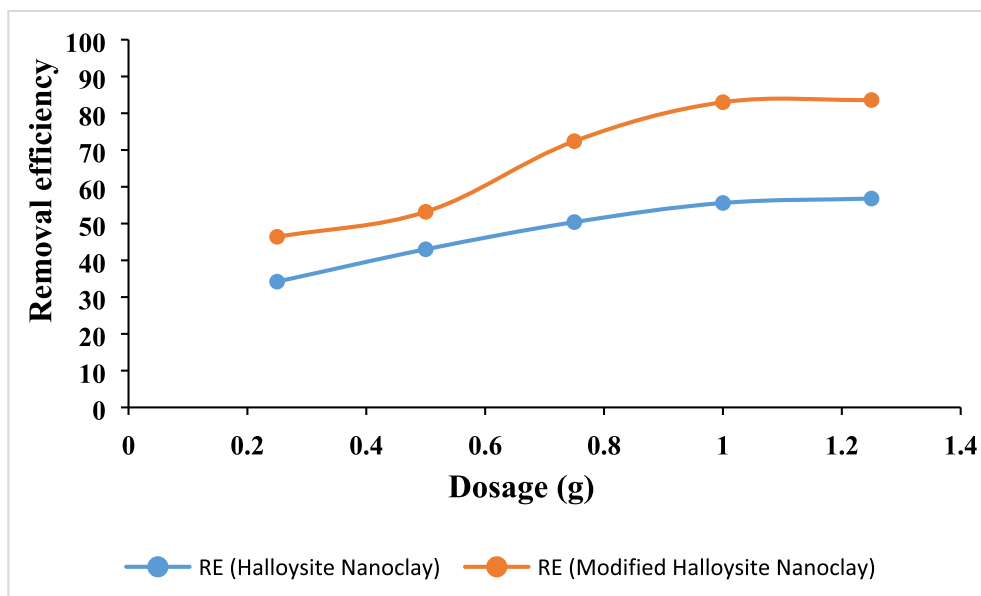


Fig. 6 The effect of HS and MHS dosage on the removal of As (III) at pH 8; Initial concentration 5 ppm; Contact time 90 min.

that the adsorption kinetics followed this model (Rahman and Haseen, 2014; Rahman et al., 2021). The MHS was found to fit well for the entire adsorption period, as evidenced by the very high correlation coefficient, as shown in the pseudo-second-order model fit in Fig. 13. Fig. 13's calculated equilibrium capacity was not showing much variations to that determined by experimental investigation (Table 2).

3.7. Isotherm studies

The isotherm study shows the efficiency of the interaction between the biosorbent and adsorbate as well as how metal ions can be dispersed across the liquid and solid phases at

different equilibrium concentrations (Maleki et al., 2015). The experimental data have been described using a variety of isotherm models, including Langmuir and Freundlich, to improve the design of the sorption system for the removal of metal ions from solutions.

In the Langmuir model, a single layer of adsorbed solute at a constant temperature is assumed together with homogeneous sorption energy. The most often used isotherm in the Langmuir model, the monolayer sorption isotherm, is expressed as follows (McRae et al., 2008):

$$q_e = \left(\frac{C_e \times Q_m \times K_L}{1 + K_L C_e} \right)$$

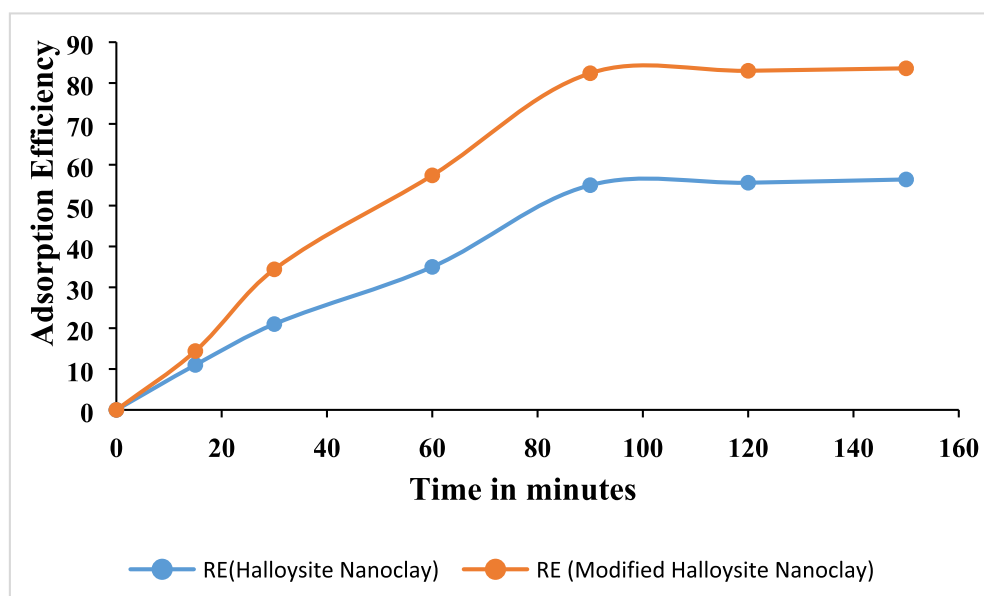


Fig. 7 The effect of contact time on the adsorption of As (III) using HS and MHS nanoclay at pH 8;; Initial concentration 5 ppm; Dosage 1 g/L.

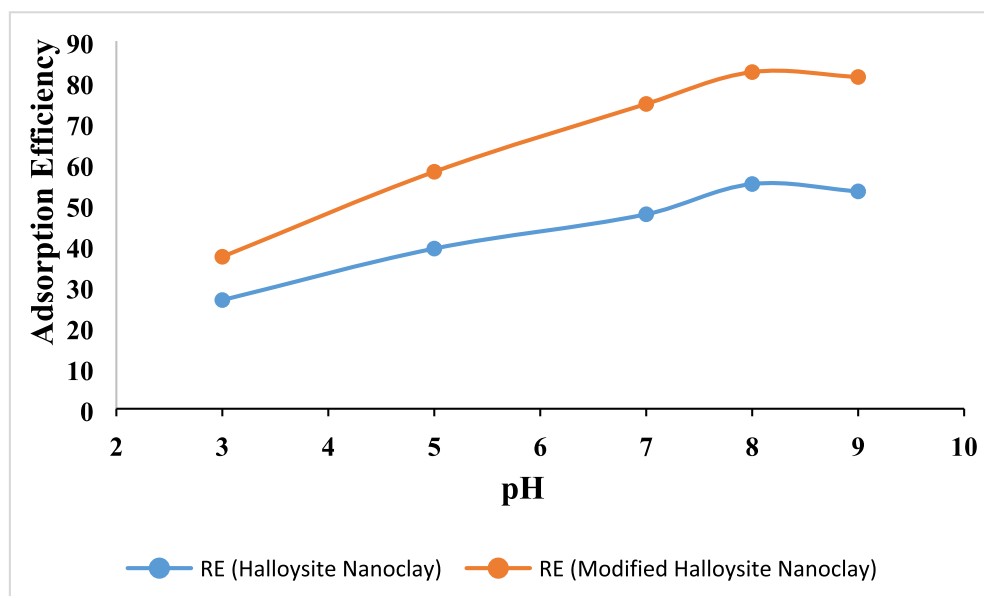


Fig. 8 The effect of solution pH on the adsorption of As (III) using HS and MHS nanoclay at Initial concentration 5 ppm; Dosage 1 g/L; Contact time 90 min.

Where q_e , C_e , Q_0 , and K_L stand for, respectively, the quantity of solute adsorbed at equilibrium (mg/g), the concentration of adsorbate at equilibrium (mg/L), the maximal adsorption capacity (mg/g), and the Langmuir constant (L/mg). The Langmuir equation's linear form is

$$\frac{C_e}{q_e} = \frac{1}{K_L Q_0} + \frac{C_e}{Q_0}$$

A linear plot of C_e/q_e against C_e was created to examine the Langmuir isotherm model's applicability for the metals adsorption onto MHS. The higher R^2 values demonstrated the Langmuir isotherm's suitability for arsenic adsorption upon MHS (Turk et al, 2020). The values of Q_0 , K_L , and R^2 (correlation coefficient) are displayed in Table3.

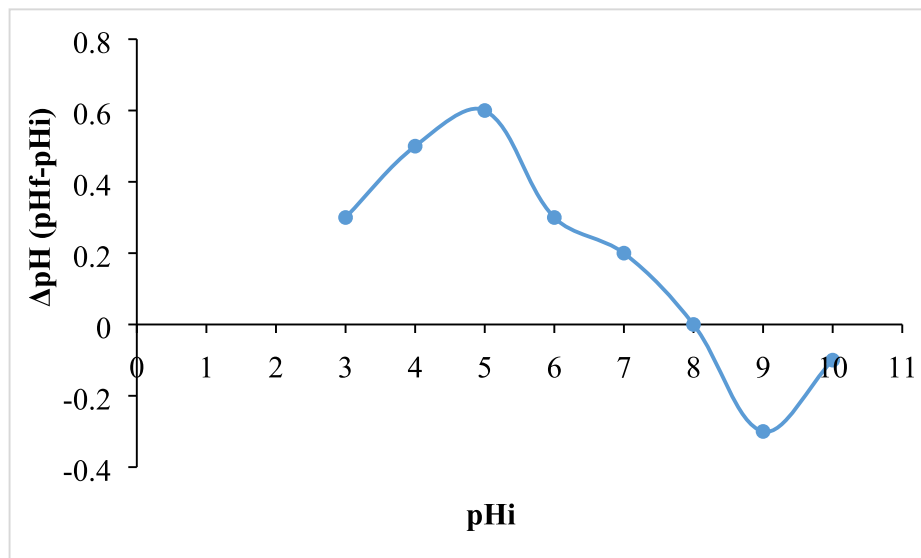


Fig. 9 Determination of point of zero charge of the adsorbent.

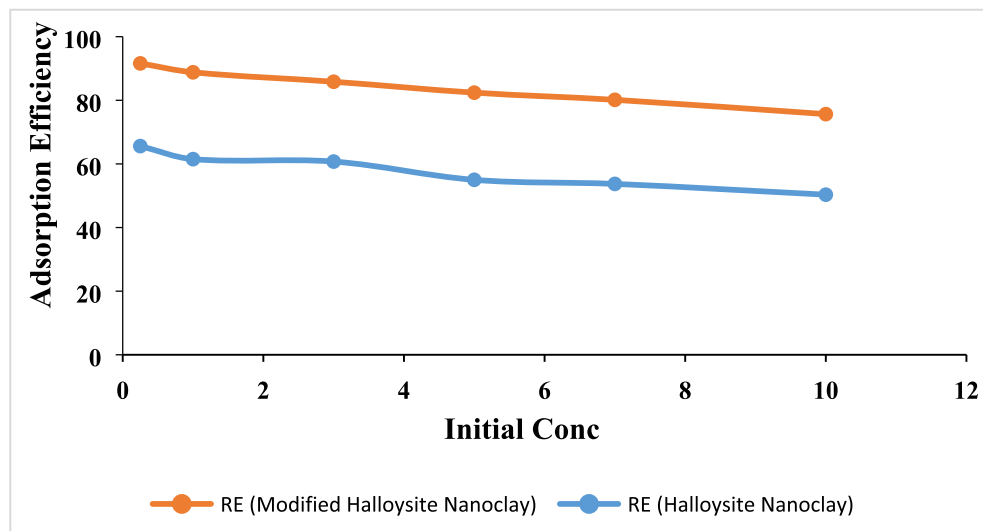


Fig. 10 The effect of initial concentration for the adsorption of As (III) at pH 8; Dosage 1 g/L; Contact time 90 min.

The Freundlich isotherm is employed in the adsorption process on heterogeneous surfaces (Akin et al. 2012). These sources provide the Freundlich isotherm equation:

$$\log Q_e = \log K_F + \frac{1}{n} \log C_e$$

Where n is the adsorption intensity and K_F is the Freundlich constant (Turk, 2017). The slope and intercept of the $\log Q_e$ against $\log C_e$ linear plot are $1/n$ and $\log K_F$, respectively. From linear graphs, the Freundlich isotherm parameters in Table 3 were derived. In these models, the correlation coefficient (R^2) was 0.98. According to Chetia et al. (2012), the K_F and n values for As (III) adsorption on MHS were determined to be 94.75 and 1.33, respectively (if $1/n$ is less than 1, adsorption is appropriate). Arsenic adsorption on MHS is

better suited by the Freundlich model, which has a higher correlation coefficient (R^2 [0.98]), however the difference between the R^2 Langmuir adsorption is very low.

3.8. Thermodynamic studies

The actual indicators for the practical application of an adsorption process are thermodynamic parameters like the Gibbs energy (ΔG), enthalpy (ΔH), and entropy (ΔS). Using the following equations [30, 37], the thermodynamic parameters were calculated:

$$\Delta G = \Delta H - T \Delta S$$

$$K_c = \frac{q_e}{C_e}$$

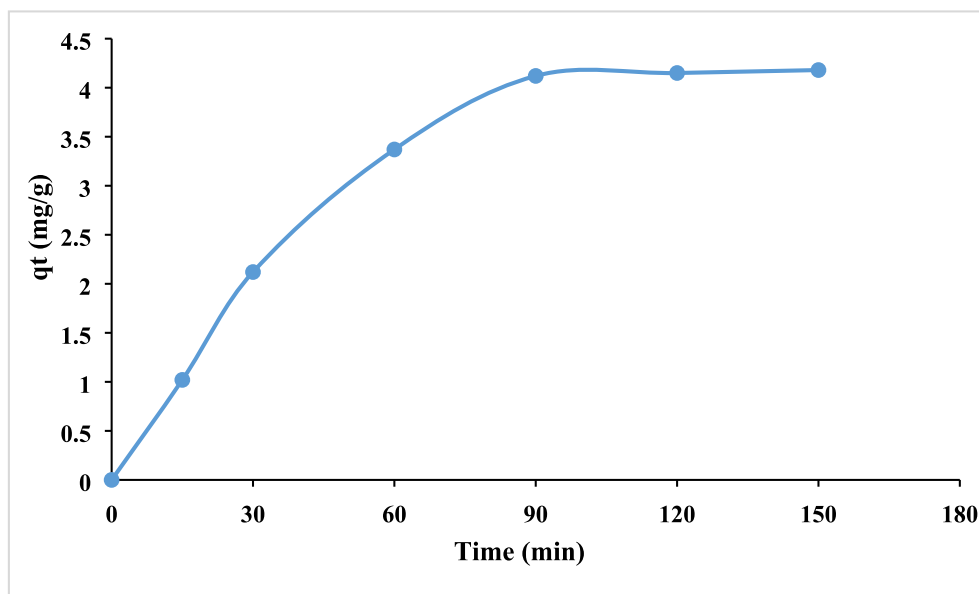


Fig. 11 The quantity of metal ions adsorbed from the desalination outfall sample by MHS nanoclay (qt).

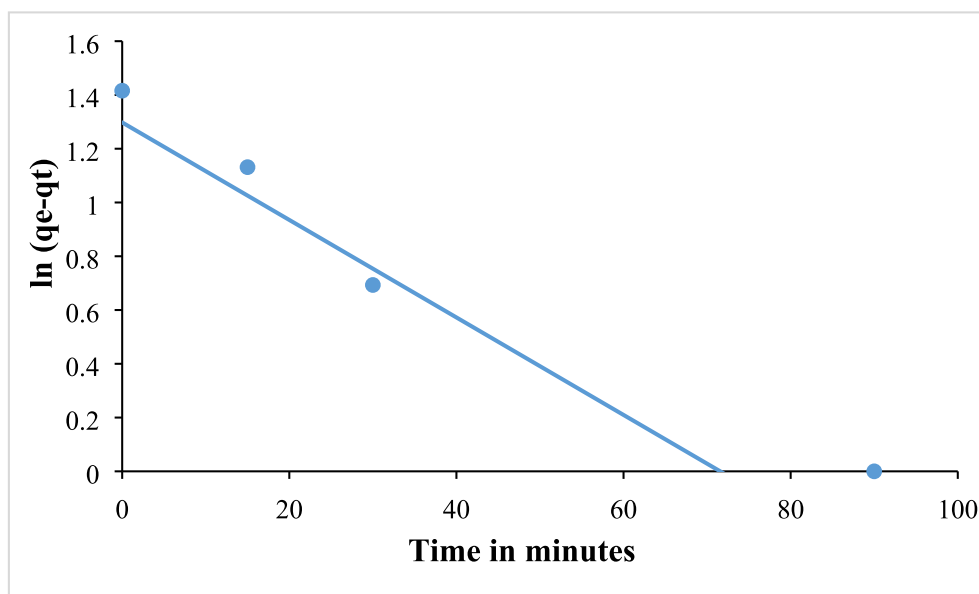


Fig. 12 The Lagergren pseudo-first-order (PFO) kinetic model.

$$\ln K_c = \frac{\Delta S}{R} - \frac{\Delta H}{RT}$$

Where K_c , q_e , C_e , R , and T are the equilibrium constants, the equilibrium quantity of metal adsorbed on the adsorbent (mol/g), the equilibrium concentration of metal in the solution (mol/L), the gas constant (8.314 J/mol K), and the absolute temperature (K), respectively. The values of ΔH and ΔS can be inferred from the slopes and intercepts of the graph of $\ln K_c$ vs $1/T$. Table 4 contains the calculated thermodynamic param-

eters. The endothermic reaction and enhanced randomization at the solid/solution interface during the adsorption of arsenic onto MHS are suggested by the positive ΔH and ΔS values. The adsorption process is implied to be spontaneous by the negative ΔG values. Additionally, the fact that ΔG values drop as temperature rises suggests that adsorption is more spontaneous at higher temperatures (Maleki et al, 2015). Additionally, MHS adsorbents' ΔG° values above -20 kJ/mol, indicating that chemisorption was the mechanism (Horsfall Jr et al. 2006).

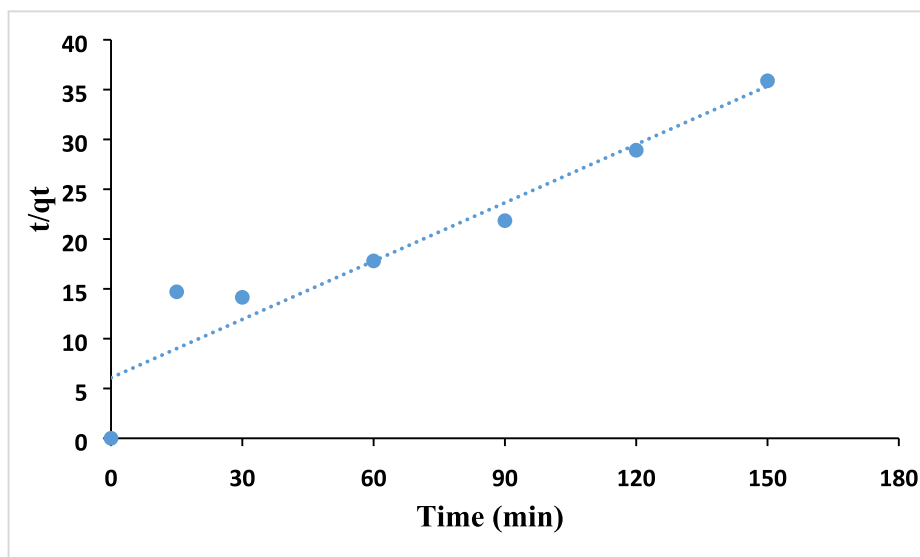


Fig. 13 The Pseudo Second Order (PSO) kinetic model (Elovich model) List of Tables.

Table 2 Pseudo-second-order isotherm parameters.

Material	q_e experimental (mg/g)	q_e calculated (mg/g)	k_2 (g/mg min)	R^2	R^2 (From pseudo-first-order)
MHS	4.12	3.55	6.07	0.91	0.82

Table 3 Linearized isotherm coefficients of arsenic adsorption by MHS.

Metal	Langmuir			Freundlich		
	Q_0	K_L	R^2	K_F	n	R^2
Arsenic	8.67	11.09	0.96	94.75	1.33	0.98

Table 4 Thermodynamic parameters of arsenic removal by MHS.

Metal	ΔH	ΔS	R^2	ΔG			
				T (K)			
				298	308	318	328
Arsenic	106.19	1.19	0.98	-222.46	-233.91	-245.36	-256.80

3.9. Comparison with other adsorbents

Due to variations in experimental circumstances and methods, it is challenging to make a direct and precise comparison between the prepared adsorbent and other studies in the literature. Table 5 compares the adsorption capacity of the developed MHS with that of other modified clay adsorbents and adsorbents with related chemical characteristics. As can be shown, compared to certain other less expensive adsor-

bents including granular ferric hydroxide, fungal biomass, and iron oxide coated sand, the MHS adsorbent material exhibits superior removal efficiency. Some of the described clays, such iron- and manganese-pillared MMT, had much lower Langmuir adsorption capabilities. The current material exhibits a comparatively higher adsorption rate and performs best at a pH that is somewhat alkaline, which is characteristic of waters that have been contaminated with arsenic (Almasri et al, 2018).

Table 5 Comparison of adsorption capacity for As (III) with other adsorbents.

Adsorbent	Adsorption capacity (mg/g)	Langmuir monolayer adsorption capacity (mg/g)	Initial concentration (mg/L)	Equilibrium time (h)	pH	Reference
Iron pillared MMT	–	0.0175	0.2–2.0	2	6	(Mishra and Mahto, 2016)
Manganese pillared MMT		0.0258	0.2–2.0	2	6	(Mishra and Mahto, 2016)
Al/Fe modified MMT	2.94	8.25	10	20	9	(Ramesh et al, 2007)
Iron oxide hydroxide nanoparticles	0.475	1.31	0.3	3	7.28	(Raul et al, 2014)
Biomass of the fungus <i>A. Niger</i> coated with iron oxide	0.075		0.1	12	6–7	(Pokhrel and Viraraghavan, 2006)
Granular ferric hydroxide	0.0475		0.1	6	7.6	Thirunavukk-arasu et al, 2003
Iron oxide coated sand	0.0183		0.325	5	7.4	Thirunavukk-arasu et al, 2001
Ferrihydrite	0.285		0.325	5	7.4	Thirunavukk-arasu et al, 2001
Hydroxyiron modified MMT	0.191	3.85	1	2	6	Almasri et al, 2018
MHS	4.12	8.67	5	1.5	8	Present study

4. Conclusion

The study was successfully implemented the application of modified Halloysite nanoclay for the effective adsorption of As (III) from the polluted water. The MHS nanoclay's physical characterization revealed that it was composed of a hollow tube-like structure. The alteration of HS nanoclay, which encourages the production of many cavities and a rather loose surface, finally led to an increase in the contact area and active sites for the adsorption of As (III) from effluents. The optimization experiments revealed the dosage of 1 g/l, pH of 8, contact time of 90 min and the initial concentration of As (III) produce the better adsorption efficiency. In the optimized condition, the current experiment produced and efficiency of 82.4 %. The outcomes showed that the pseudo-second-order model was the most suitable for the adsorption of As (III) from the polluted water due the theoretical and experimental sorption capacities were in excellent agreement. The Freundlich model, which has a stronger correlation coefficient (0.98), is better suited to describe arsenic adsorption on MHS; nonetheless, the difference between the R^2 Langmuir adsorption (0.96) is relatively small. The present study light on the extension of the work with the doping of nanosized semiconductor with the prepared HS nanoclay to make better degradation of various organic and inorganic contaminants from contaminated water by means of photocatalysis.

Declaration of Competing Interest

The authors declare that they have no known competing financial interests or personal relationships that could have appeared to influence the work reported in this paper.

Acknowledgement

All the authors are greatly thankful to the Department of Marine Chemistry, Chemistry and Environmental Science for the technical support.

References

- Abdel-Fadeel, M.A., Aljohani, N.S., Al-Mhyawi, S.R., Halawani, R. F., Aljuhani, E.H., Salam, M.A., 2022. A simple method for removal of toxic dyes such as Brilliant Green and Acid Red from the aquatic environment using Halloysite nanoclay. *J. Saudi Chem. Soc.* 26, (3) 101475.
- Aigbe, U.O., Ukhurebor, K.E., Onyancha, R.B., Okundaye, B., Pal, K., Osibote, O.A., Esiekepe, E.L., Kusuma, H.S. and Darmokoesomo, H., 2022. A facile review on the sorption of heavy metals and dyes using bionanocomposites. *Adsorption Science & Technology*, 2022.
- Akin, I., Arslan, G., Tor, A., Ersoz, M., Cengeloglu, Y., 2012. Arsenic (V) removal from underground water by magnetic nanoparticles synthesized from waste red mud. *J. Hazard. Mater.* 235, 62–68.
- Alfarawati, R.K., Shaban, Y.A., Turki, A.J., Kavil, Y.N., Zobidi, M. I., 2020. Solar photocatalytic removal of arsenic from polluted water using carbon-modified titanium oxide nanoparticles supported on activated carbon. *Environ. Chem.* 17 (8), 568–578.
- Aljohani, N.S., Al-Farawati, R.K., Shabbaj, I.I., Al-Mur, B.A., Kavil, Y.N., Abdel Salam, M., 2021. Environmental remediation of desalination plant outfall brine discharge from heavy metals and salinity using halloysite nanoclay. *Water* 13 (7), 969.
- Alley, E.R., 2007. *Water quality control handbook*. McGraw-Hill Education.
- Almasri, D.A., Rhadfi, T., Atieh, M.A., McKay, G., Ahzi, S., 2018. High performance hydroxyiron modified montmorillonite nanoclay adsorbent for arsenite removal. *Chem. Eng. J.* 335, 1–12.
- Asere, T.G., Stevens, C.V., Du Laing, G., 2019. Use of (modified) natural adsorbents for arsenic remediation: a review. *Sci. Total Environ.* 676, 706–720.
- Attia, A.A., Khedr, S.A., Elkholy, S.A., 2010. Adsorption of chromium ion (VI) by acid activated carbon. *Braz. J. Chem. Eng.* 27, 183–193.
- Azouaou, N., Sadaoui, Z., Djaafri, A., Mokaddem, H., 2010. Adsorption of cadmium from aqueous solution onto untreated coffee grounds: Equilibrium, kinetics and thermodynamics. *J. Hazard. Mater.* 184 (1–3), 126–134.

- Babel, S., Kurniawan, T.A., 2003. Low-cost adsorbents for heavy metals uptake from contaminated water: a review. *J. Hazard. Mater.* 97 (1–3), 219–243.
- Bakatula, E.N., Richard, D., Neculita, C.M., Zagury, G.J., 2018. Determination of point of zero charge of natural organic materials. *Environmental Science and Pollution Research* 25, 7823–7833.
- Bhattacharyya, K.G., Gupta, S.S., 2008. Adsorption of a few heavy metals on natural and modified kaolinite and montmorillonite: a review. *Adv. Colloid Interface Sci.* 140 (2), 114–131.
- Bhowmick, S., Chakraborty, S., Mondal, P., Van Renterghem, W., Van den Berghe, S., Roman-Ross, G., Chatterjee, D., Iglesias, M., 2014. Montmorillonite-supported nanoscale zero-valent iron for removal of arsenic from aqueous solution: Kinetics and mechanism. *Chem. Eng. J.* 243, 14–23.
- Brahmaiah, T., Spurthi, L., Chandrika, K., Ramanaiah, S., Prasad, K. S., 2015. Kinetics of heavy metal (Cr & Ni) removal from the wastewater by using low cost adsorbent. *World J. Pharm. Pharma. Sci.* 4 (11), 1600–1610.
- Chakraborty, R., Asthana, A., Singh, A.K., Jain, B., Susan, A.B.H., 2022. Adsorption of heavy metal ions by various low-cost adsorbents: a review. *Int. J. Environ. Anal. Chem.* 102 (2), 342–379.
- Chalasan, R., Vasudevan, S., 2012. Cyclodextrin functionalized magnetic iron oxide nanocrystals: a host-carrier for magnetic separation of non-polar molecules and arsenic from aqueous media. *J. Mater. Chem.* 22 (30), 14925–14931.
- Chetia, M., Goswamee, R.L., Banerjee, S., Chatterjee, S., Singh, L., Srivastava, R.B., Sarma, H.P., 2012. Arsenic removal from water using calcined Mg–Al layered double hydroxide. *Clean Techn. Environ. Policy* 14 (1), 21–27.
- Ciopec, M., Davidescu, C.M., Negrea, A., Lupa, L., Popa, A., Muntean, C., Ardelean, R., Ilia, G., 2013. Synthesis, characterization, and adsorption behavior of aminophosphinic grafted on poly (styrene-co-divinylbenzene) for divalent metal ions in aqueous solutions. *Polym. Eng. Sci.* 53 (5), 1117–1124.
- Costa, M., 2019. Review of arsenic toxicity, speciation and polyadenylation of canonical histones. *Toxicol. Appl. Pharmacol.* 375, 1–4.
- Crini, G., Gimbert, F., Robert, C., Martel, B., Adam, O., Morin-Crini, N., De Giorgi, F., Badot, P.M., 2008. The removal of Basic Blue 3 from aqueous solutions by chitosan-based adsorbent: batch studies. *J. Hazard. Mater.* 153 (1–2), 96–106.
- Du, Y.J., Wei, M.L., Reddy, K.R., Jin, F., Wu, H.L., Liu, Z.B., 2014. New phosphate-based binder for stabilization of soils contaminated with heavy metals: leaching, strength and microstructure characterization. *Journal of Environmental Management* 146, 179–188.
- Ghaemy, M., Shabzendedar, S., Taghavi, M., 2015. Synthesis and characterization of heterocyclic functionalized polymers by click reaction: Preparation of magnetic nanocomposites and studies on their thermal, mechanical, photophysical and metal ions removal properties. *Chinese Journal of Polymer Science* 33, 301–317.
- Han, M.J., Hao, J., Christodoulatos, C., Korfiatis, G.P., Wan, L.J., Meng, X., 2007. Direct evidence of arsenic (III)–carbonate complexes obtained using electrochemical scanning tunneling microscopy. *Anal. Chem.* 79 (10), 3615–3622.
- Ho, Y.S., McKay, G., 1998. Sorption of dye from aqueous solution by peat. *Chem. Eng. J.* 70 (2), 115–124.
- Horsfall Jr, M., Abia, A.A., Spiff, A.I., 2006. Kinetic studies on the adsorption of Cd²⁺, Cu²⁺ and Zn²⁺ ions from aqueous solutions by cassava (*Manihot sculenta* Cranz) tuber bark waste. *Bioresour. Technol.* 97 (2), 283–291.
- Kavil, Y.N., Shaban, Y.A., Orif, M.I., Al-Farawati, R., Zobidi, M., Khan, S.U., 2018. Production of methanol as a fuel energy from CO₂ present in polluted seawater—a photocatalytic outlook. *Open Chem.* 16 (1), 1089–1098.
- Kavil, Y.N., Shaban, Y.A., Alelyani, S.S., Al-Farawati, R., Orif, M.I., Ghandourah, M.A., Schmidt, M., Turki, A.J., Zobidi, M., 2020. The removal of methylene blue as a remedy of dye-based marine pollution: a photocatalytic perspective. *Res. Chem. Intermed.* 46 (1), 755–768.
- Kosa, S.A., Al-Zhrani, G., Salam, M.A., 2012. Removal of heavy metals from aqueous solutions by multi-walled carbon nanotubes modified with 8-hydroxyquinoline. *Chem. Eng. J.* 181, 159–168.
- Kumar, P.S., Ramalingam, S., Senthamarai, C., Niranjana, M., Vijayalakshmi, P., Sivanesan, S., 2010. Adsorption of dye from aqueous solution by cashew nut shell: studies on equilibrium isotherm, kinetics and thermodynamics of interactions. *Desalination* 261 (1–2), 52–60.
- Long, H., Wu, P., Zhu, N., 2013. Evaluation of Cs⁺ removal from aqueous solution by adsorption on ethylamine-modified montmorillonite. *Chem. Eng. J.* 225, 237–244.
- Maleki, A., Pajootan, E., Hayati, B., 2015. Ethyl acrylate grafted chitosan for heavy metal removal from wastewater: equilibrium, kinetic and thermodynamic studies. *J. Taiwan Inst. Chem. Eng.* 51, 127–134.
- Manna, S., Roy, D., Adhikari, B., Thomas, S., Das, P., 2018. Biomass for water defluoridation and current understanding on biosorption mechanisms: a review. *Environ. Prog. Sustain. Energy* 37 (5), 1560–1572.
- Martinez, M.L., Torres, M.M., Guzman, C.A., Maestri, D.M., 2006. Preparation and characteristics of activated carbon from olive stones and walnut shells. *Ind. Crop. Prod.* 23 (1), 23–28.
- McRae, R.L., Phillips, R.L., Kim, I.B., Bunz, U.H., Fahrni, C.J., 2008. Molecular recognition based on low-affinity polyvalent interactions: selective binding of a carboxylated polymer to fibronectin fibrils of live fibroblast cells. *J. Am. Chem. Soc.* 130 (25), 7851–7853.
- Mishra, T., Mahato, D.K., 2016. A comparative study on enhanced arsenic (V) and arsenic (III) removal by iron oxide and manganese oxide pillared clays from ground water. *J. Environ. Chem. Eng.* 4 (1), 1224–1230.
- Mohan, D., Pittman Jr, C.U., 2007. Arsenic removal from water/wastewater using adsorbents—a critical review. *J. Hazard. Mater.* 142 (1–2), 1–53.
- Montazer-Rahmati, M.M., Rabbani, P., Abdolali, A., Keshtkar, A.R., 2011. Kinetics and equilibrium studies on biosorption of cadmium, lead, and nickel ions from aqueous solutions by intact and chemically modified brown algae. *J. Hazard. Mater.* 185 (1), 401–407.
- Negrea, A., Popa, A., Ciopec, M., Lupa, L., Negrea, P., Davidescu, C. M., Motoc, M., Minzatu, V., 2014. Phosphonium grafted styrene-divinylbenzene resins impregnated with iron (III) and crown ethers for arsenic removal. *Pure Appl. Chem.* 86 (11), 1729–1740.
- Novikau, R., Lujaniene, G., 2022. Adsorption behaviour of pollutants: Heavy metals, radionuclides, organic pollutants, on clays and their minerals (raw, modified and treated): a review. *J. Environ. Manage.* 309, 114685.
- Orif, M.I., Kavil, Y.N., Kelassanthodi, R., Al-Farawati, R., Zobidi, M.I.A., 2017. Dissolved methane and oxygen depletion in the two coastal lagoons, Red Sea. *Indian. Journal of Geo-Marine Sciences* 46 (7), 1287–1297.
- Park, D., Yun, Y.S., Park, J.M., 2010. The past, present, and future trends of biosorption. *Biotechnol. Bioprocess Eng.* 15 (1), 86–102.
- Peechattukudy, L.A., Dhoble, R.M., 2017. Removal of nitrate from water by adsorption—a review. *IJSTE-Int. J. Sci. Technol. Eng.* 3 (09).
- Pokhrel, D., Viraraghavan, T., 2006. Arsenic removal from an aqueous solution by a modified fungal biomass. *Water Res.* 40 (3), 549–552.

- Rahman, N., Haseen, U., 2014. Equilibrium modeling, kinetic, and thermodynamic studies on adsorption of Pb (II) by a hybrid inorganic-organic material: polyacrylamide zirconium (IV) iodate. *Ind. Eng. Chem. Res.* 53 (19), 8198–8207.
- Rahman, N., Nasir, M., Alothman, A.A., Al-Enizi, A.M., Ubaidullah, M., Shaikh, S.F., 2021. Synthesis of 2-mercaptopropionic acid/hydrous zirconium oxide composite and its application for removal of Pb (II) from water samples: central composite design for optimization. *J. King Saud Univ.-Sci.* 33, (2) 101280.
- Rahman, N., Raheem, A., 2022. Fabrication of graphene oxide/inulin impregnated with ZnO nanoparticles for efficient removal of enrofloxacin from water: taguchi-optimized experimental analysis. *J. Environ. Manage.* 318, 115525.
- Rahman, N., Varshney, P., 2021. Effective removal of doxycycline from aqueous solution using CuO nanoparticles decorated poly (2-acrylamido-2-methyl-1-propanesulfonic acid)/chitosan. *Environmental Science and Pollution Research* 28, 43599–43617.
- Rahman, N., Varshney, P., Nasir, M., 2021. Synthesis and characterization of polydopamine/hydrous zirconium oxide composite and its efficiency for the removal of uranium (VI) from water. *Environ. Nanotechnol. Monit. Manage.* 15, 100458.
- Ramesh, A., Hasegawa, H., Maki, T., Ueda, K., 2007. Adsorption of inorganic and organic arsenic from aqueous solutions by polymeric Al/Fe modified montmorillonite. *Sep. Purif. Technol.* 56 (1), 90–100.
- Raul, P.K., Devi, R.R., Umlong, I.M., Thakur, A.J., Banerjee, S., Veer, V., 2014. Iron oxide hydroxide nanoflower assisted removal of arsenic from water. *Mater. Res. Bull.* 49, 360–368.
- Rodriguez-Narvaez, O.M., Peralta-Hernandez, J.M., Goonetilleke, A., Bandala, E.R., 2017. Treatment technologies for emerging contaminants in water: a review. *Chem. Eng. J.* 323, 361–380.
- Selomulya, C., Meeyoo, V., Amal, R., 1999. Mechanisms of Cr (VI) removal from water by various types of activated carbons. *J. Chem. Technol. Biotechnol.: Int. Res. Process, Environ. Clean Technol.* 74 (2), 111–122.
- Senoussi, H., Osmani, H., Courtois, C. and el Hadi Bourahli, M., 2016. Mineralogical and chemical characterization of DD3 kaolin from the east of Algeria. *boletín de la sociedad española de cerámica y vidrio*, 55(3), pp.121-126.
- Shaban, Y.A., 2019. Solar light-induced photodegradation of chrysene in seawater in the presence of carbon-modified n-TiO₂ nanoparticles. *Arab. J. Chem.* 12 (5), 652–663.
- Shao, Q., Wang, T., Wang, X., Chen, Y., 2011. Bis-(8-hydroxyquinoline) copper nanoribbons: preparation, characterization, and photoconductivity. *Front. Optoelectron. China* 4 (2), 195–198.
- Sharma, S., Bhattacharya, A., 2017. Drinking water contamination and treatment techniques. *Appl. Water Sci.* 7 (3), 1043–1067.
- Singh, N., Singh, S.P., Gupta, V., Yadav, H.K., Ahuja, T., Tripathy, S.S., 2013. A process for the selective removal of arsenic from contaminated water using acetate functionalized zinc oxide nanomaterials. *Environ. Prog. Sustain. Energy* 32 (4), 1023–1029.
- Tandon, P.K., Shukla, R.C., Singh, S.B., 2013. Removal of arsenic (III) from water with clay-supported zerovalent iron nanoparticles synthesized with the help of tea liquor. *Ind. Eng. Chem. Res.* 52 (30), 10052–10058.
- Thirunavukkarasu, O.S., Viraraghavan, T., Subramanian, K.S., 2001. Removal of arsenic in drinking water by iron oxide-coated sand and ferrihydrite—batch studies. *Water Qual. Res. J.* 36 (1), 55–70.
- Thirunavukkarasu, O.S., Viraraghavan, T., Subramanian, K.S., 2003. Arsenic removal from drinking water using granular ferric hydroxide. *Water SA* 29 (2), 161–170.
- Thommes, M., 2010. Physical adsorption characterization of nanoporous materials. *Chem. Ing. Tech.* 82 (7), 1059–1073.
- Türk, T., 2017. Removal of dissolved arsenic by pyrite ash waste. *Mine Water Environ* 36, 255–263.
- Türk, T., Boyraz, T., Alp, İ., 2020. Arsenic removal from groundwater in Kütahya, Turkey, by novel calcined modified hydrotalcite. *Environmental geochemistry and health* 42, 1335–1345.
- Ushakumary, E.R., Madhu, G., 2013. Waste water treatment using low cost natural adsorbents (Doctoral dissertation. Cochin University Of Science And Technology).
- Weber Jr, W.J., Morris, J.C., 1963. Kinetics of adsorption on carbon from solution. *J. Sanit. Eng. Div.* 89 (2), 31–59.
- Weerasuriya, D.R.K., Wijesinghe, W.P.S.L., Rajapakse, R.M.G., 2017. Encapsulation of anticancer drug copper bis (8-hydroxyquinoline) in hydroxyapatite for pH-sensitive targeted delivery and slow release. *Mater. Sci. Eng. C* 71, 206–213.
- Wen, Y., Ji, Y., Zhang, S., Zhang, J., Cai, G., 2019. A simple low-cost method to prepare lignocellulose-based composites for efficient removal of Cd (II) from wastewater. *Polymers* 11 (4), 711.
- WHO, 2006. Guidelines for drinking-water quality [electronic resource]: incorporating first addendum.
- Yagub, M.T., Sen, T.K., Afroze, S., Ang, H.M., 2014. Dye and its removal from aqueous solution by adsorption: a review. *Adv. Colloid Interface Sci.* 209, 172–184.
- Yuh-Shan, H., 2004. Citation review of Lagergren kinetic rate equation on adsorption reactions. *Scientometrics* 59 (1), 171–177.
- Zhang, X., Wang, X., 2015. Adsorption and desorption of nickel (II) ions from aqueous solution by a lignocellulose/montmorillonite nanocomposite. *PLoS One* 10 (2), e0117077.
- Zhu, R., Chen, Q., Zhou, Q., Xi, Y., Zhu, J., He, H., 2016. Adsorbents based on montmorillonite for contaminant removal from water: a review. *Appl. Clay Sci.* 123, 239–258.